

Scaling properties of a spatial one-particle density-matrix entropy in many-body localized systems

Miroslav Hopjan,¹ Fabian Heidrich-Meisner,¹ and Vincenzo Alba²

¹*Institut für Theoretische Physik, Georg-August-Universität Göttingen,
Friedrich-Hund-Platz 1, 37077 Göttingen, Germany*

²*Institute for Theoretical Physics, Universiteit van Amsterdam,
Science Park 904, Postbus 94485, 1098 XH Amsterdam, The Netherlands*

We investigate a spatial subsystem entropy extracted from the one-particle density matrix (OPDM) of one-dimensional disordered interacting fermions that host a many-body localized (MBL) phase. Deep in the putative MBL regime, this OPDM entropy exhibits the salient scaling features of localization, even though it provides only an upper bound to the von-Neumann entropy. First, we numerically show that the OPDM entropy of the eigenstates obeys an area law. Second, similar to the von-Neumann entropy, the OPDM entropy grows logarithmically with time after a quantum quench, albeit with a different prefactor. Both these features survive at moderately large interactions and well towards the transition into the ergodic phase. We discuss prospects for calculating the OPDM entropy using approximate numerical methods and for its measurement in quantum-gas experiments.

I. INTRODUCTION

Many-body localized (MBL) systems challenge the usual paradigm of thermalization [1–5]. While it is well-established that for non-interacting particles, disorder leads to Anderson localization [6], it has been suggested that for sufficiently strong disorder, a localized phase survives in the presence of interactions [7, 8]. Despite intense theoretical effort (see recent reviews [1–5]), the scenario is not fully settled. On the experimental side, MBL has been investigated in trapped ions [9], ultracold atoms [10–14], or superconducting qubits [15–18]. Experimental signatures of MBL have been observed in the quasiperiodic Aubry-André Fermi-Hubbard model [11, 19], the disordered Ising model [9], the disordered Bose-Hubbard model (BHM) [10, 14], and the quasiperiodic Aubry-André Bose-Hubbard model [12, 13].

Entanglement-related measures, such as the von-Neumann entropy, display several intriguing behaviors in the putative MBL phase. First, a distinctive feature of localization is that eigenstates exhibit area-law entanglement [20–22], in stark contrast with the volume law expected in clean systems. Second, the entanglement entropy grows logarithmically after global quenches [23–26], which is regarded as a “smoking gun” evidence for MBL. Indeed, this is different in Anderson-localized systems, where the entanglement entropy saturates, and in clean systems, where a linear behavior occurs, rigorously established for integrable models [27–30]. The logarithmic growth can be explained by the existence of emergent local integrals of motion in the MBL phase [25, 31–33]. Remarkably, the logarithmic growth of the entanglement entropy has been observed in cold-atom experiments [13] and systems of superconducting qubits [15, 17]. However, measuring entanglement is a challenging task and cannot easily be scaled up to larger systems, as it requires full quantum state tomography [15], accessing all the n -point correlation functions [13, 17], or a high-fidelity state

preparation [13].

Here, we show that a suitably defined spatial-subsystem entropy based on the *one-particle density matrix* (OPDM) computed in eigenstates and its out-of-equilibrium dynamics after a quantum quench contains salient information about MBL phases, akin to the behavior of the spatial entanglement entropy. The main motivation for studying the OPDM is that in the MBL phase, the eigenstates of the OPDM are localized in real space but delocalized in the ergodic phase [34, 35]. Moreover, its eigenvalues indicate Fock-space localization in the MBL regime [34, 35], a defining feature of MBL [8, 36–38]. This is reflected in the OPDM being close to that of a free-fermion system [34, 35, 39–43], and its eigenmodes being a proxy for the localized quasiparticles [35].

We focus on the OPDM restricted to a subsystem A and on the associated entropy. For non-interacting fermionic systems, this coincides with the von-Neumann entropy [44, 45]. We consider a generic model of disordered spinless fermions with nearest-neighbor interactions. Numerically, we show that in the MBL phase, the disorder-averaged OPDM entropy exhibits an area law in eigenstates, similar to the von-Neumann entropy. This is remarkable because in the presence of interactions, the OPDM entropy is not a proper (spatial) entanglement measure.

Crucially, after a quantum quench in the MBL phase, the OPDM entropy increases logarithmically with time, similar to the von-Neumann entropy. The prefactor of the logarithmic growth is non-universal, and it is different from that of the von-Neumann entropy. The logarithmic growth survives for moderately strong interactions and as the disorder strength is decreased. In the non-interacting limit, i.e., for the Anderson insulator, the OPDM entropy saturates. Our results establish the OPDM entropy as an alternative diagnostic tool for the MBL phase. This could be relevant for both experiments and approximate theoretical approaches inspired by ab-initio methods. Im-

portantly, provided that one has access to the correlation function [46], the computational cost of extracting the OPDM entropy from the correlation function is only polynomial. We also note that the OPDM diagnostic tool that we propose is not limited to the regime of weak interactions, in contrast with other one-body measures based on Anderson orbitals [47] or the self-consistent Hartree-Fock approximation [48].

The plan of the paper is following: In Sec. II, we introduce a model of spinless fermions with a nearest-neighbor interaction and provide basic definitions. The OPDM entropy will be introduced in Sec. III. In Sec. IV, we provide details of the numerical simulations. The distributions of the OPDM entropy for our model are discussed in Sec. V. We then numerically demonstrate that the disorder-averaged OPDM entropy satisfies an area law in Sec. VI. Finally, we show in Sec. VII that the disorder-averaged OPDM entropy increases logarithmically in time in global quenches from product states. We conclude in Sec. VIII.

II. MODEL AND DEFINITIONS

In this paper, we consider spinless fermions with a nearest-neighbor interaction and with diagonal disorder described by the Hamiltonian

$$H = \sum_{i=1}^L \left[-\frac{J}{2}(c_i^\dagger c_{i+1} + h.c.) + V(n_i - 1/2)(n_{i+1} - 1/2) + \epsilon_i(n_i - 1/2) \right], \quad (1)$$

where $c_i^{(\dagger)}$ is a fermionic creation/annihilation operator and $n_i = c_i^\dagger c_i$ is the fermionic density at site i . L is the system size, J is the hopping matrix element, V is the strength of the nearest-neighbor interactions, and ϵ_i is a random potential drawn from a uniform box distribution $[-W, W]$. Using a Jordan-Wigner transformation, Eq. (1) can be mapped onto a spin-1/2 XXZ chain with random local magnetic fields. For $V/J = 1$, one obtains the isotropic Heisenberg model which is a standard system where MBL physics has been investigated [5, 36]. Here, we consider $V/J = 1$ and $V/J = 0.1$ as representative of the strong and weak interactions regime, respectively.

We will compare the behavior of the OPDM entropy to that of the von-Neumann entanglement entropy $S_{\text{vN}}(A)$ of a subsystem A . First, we split the system into two parts, A and its complement \bar{A} . We always consider the case in which A and \bar{A} are equal to the half chain. Any state of the full system $|\psi\rangle$ can be Schmidt-decomposed as

$$|\psi\rangle = \sum_{\mu} \sqrt{\lambda_{\mu}} |\phi_{\mu}\rangle_A |\varphi_{\mu}\rangle_{\bar{A}}, \quad (2)$$

where the $\sqrt{\lambda_{\mu}}$ are the Schmidt coefficients and $\{|\phi_{\mu}\rangle_A\}$ and $\{|\varphi_{\mu}\rangle_{\bar{A}}\}$ are orthonormal bases for A and \bar{A} . The

von-Neumann entanglement entropy is given by

$$S_{\text{vN}}(A) = - \sum_{\mu} \lambda_{\mu} \ln \lambda_{\mu}. \quad (3)$$

For a pure state $|\psi\rangle$, Eq. (2) implies that $S_{\text{vN}}(A) = S_{\text{vN}}(\bar{A})$.

III. OPDM ENTROPY

Our main interest is in the properties of an entropy extracted from the one-particle density matrix (OPDM): We restrict the OPDM $\rho_{ij}^{(1)} = \langle \psi | c_i^\dagger c_j | \psi \rangle$ ($1 \leq i, j \leq L$) to a subsystem A , which yields

$$C_{ij}^{(A)} = \langle \psi | c_i^\dagger c_j | \psi \rangle, \quad i, j \in A, \quad (4)$$

where $|\psi\rangle$ is a many-body state. $C^{(A)}$ is usually called correlation matrix. Given the eigenvalues n_{α} of $C^{(A)}$, we define the OPDM entropy as

$$S_{\text{OPDM}}(A) = - \sum_{\alpha} (n_{\alpha} \ln(n_{\alpha}) + (1 - n_{\alpha}) \ln(1 - n_{\alpha})). \quad (5)$$

Even though we restricted the OPDM to a subsystem, we use the name OPDM entropy for simplicity. The OPDM entropy defined here should not be confused with the entanglement of one particle with all other ones [34, 35, 49]. For non-interacting fermions, S_{OPDM} coincides with the von-Neumann entropy [44, 45] because the reduced density matrix of system A is a Gaussian operator, which is fully characterized by the correlation matrix $C^{(A)}$. Indeed, the entanglement entropy of a generic Gaussian state with correlation matrix $C^{(A)}$ is given by Eq. (5).

Several remarks are in order. First, it is instructive to consider the case where A is the full system. Clearly, in this case, $S_{\text{vN}} = 0$ holds. For a free fermion system, the eigenvalues n_{α} of the OPDM are the fermionic occupations of the single-particle orbitals and $n_{\alpha} = 0, 1$, with $\sum_{\alpha} n_{\alpha} = N$, where N the total number of fermions. By using (5), this implies that the full-system OPDM entropy is zero. In the presence of interactions, this is not the case for the OPDM entropy. Specifically, upon switching on interactions, yet still in the MBL regime, the eigenvalues of the OPDM exhibit a bimodal distribution with $n_{\alpha} \approx 0, 1$, signaling that the true eigenmodes are quasiparticles. Therefore, the full-system OPDM entropy of an interacting system is non-zero except in trivial limiting cases.

While the previous argument holds for A being the full system, in fact, S_{OPDM} always upper-bounds S_{vN} . This can be seen from considering a generic fermionic state and an arbitrary partitioning. Indeed, it has been shown that given the set of fermionic states with a fixed matrix $C^{(A)}$ [cf. (4)], the Gaussian states maximize the von-Neumann entropy [50]. (A similar result holds for bosonic states [51, 52]. The proof relies only on the strong

subadditivity of the von-Neumann entropy, on the invariance under local unitary operations, and its additivity for tensor-product density matrices.) This implies that generic fermionic states, such as eigenstates of interacting many-body systems, have lower values of S_{vN} than the corresponding Gaussian state with the same correlation matrix $C^{(A)}$. The OPDM approximation, Eq. (5), applied to an arbitrary state of an interacting system, projects onto the von-Neumann entropy of the corresponding Gaussian state, which is then necessarily larger than the true S_{vN} . This holds true both for eigenstates and the out-of-equilibrium dynamics, meaning that at any time, one has $S_{\text{OPDM}}(t) \geq S_{\text{vN}}(t)$.

In the following sections, we show that the OPDM entropy exhibits two of the hallmark features of MBL, namely the area-law behavior in excited states and the logarithmic growth after a global quantum quench.

IV. NUMERICAL METHOD FOR OBTAINING EIGENSTATES

We use exact diagonalization to compute all eigenstates of (1) up to $L = 18$. We consider a system with periodic boundary conditions, and we restrict ourselves to a fixed number of fermions $N/L = 1/2$, which corresponds to zero magnetization in the spin language. We average the OPDM entropy over 10^4 disorder realizations for $L \leq 16$ and 10^3 disorder realizations for $L = 18$. We focus on entanglement properties of mid-spectrum eigenstates. Precisely, for each disorder realization, we consider eigenstates with an energy such that $\epsilon = (E - E_{\text{min}})/(E_{\text{max}} - E_{\text{min}}) \approx 1/2$, with E_{min} the ground-state energy and E_{max} the energy of the most excited state. We use the shift-and-invert method [53] to target the desired energy window. Typically, for each disorder realization, we consider 6 eigenstates.

V. DISTRIBUTION OF S_{OPDM}

Throughout the paper, we consider the bipartition where A and \bar{A} have the same length of $L/2$. For such a partitioning we always observe that both S_{OPDM} and S_{vN} lie within the interval $[0, L/2 \log(2)]$. Moreover, for maximally entangled states, we observe $S_{\text{OPDM}} = S_{\text{vN}} = L/2 \ln(2)$ whereas for product states (that have no entanglement), $S_{\text{OPDM}} = S_{\text{vN}} = 0$ (see the discussion below). An important observation is that in the presence of interactions and disordered, $S_{\text{OPDM}}(A) \neq S_{\text{OPDM}}(\bar{A})$. This asymmetry is induced by disorder, yet for the disorder average, $\bar{S}_{\text{OPDM}}(A) \approx \bar{S}_{\text{OPDM}}(\bar{A})$.

Next, we study the full distribution of $S_{\text{OPDM}}(A)$ and $S_{\text{OPDM}}(\bar{A})$, shown in Figs. 1(a) and (b), where the distribution of S_{vN} is also included. At small values of S_{OPDM} , $P(S_{\text{OPDM}}(A)) \approx P(S_{\text{vN}})$ while both $P(S_{\text{OPDM}}(A))$ and $P(S_{\text{OPDM}}(\bar{A}))$ exhibit significant tails beyond the largest values of S_{vN} . For this reason, we introduce $S_{\text{OPDM}}^{\text{min}}$ and

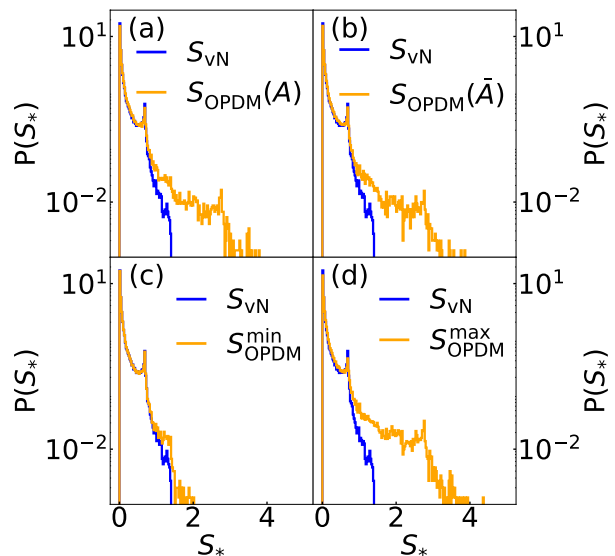


FIG. 1. (a), (b) Eigenstate distribution P of $S_{\text{OPDM}}(A)$ and $S_{\text{OPDM}}(\bar{A})$, respectively. The distribution $P(S_{\text{vN}})$ (dark-shaded area) is also included. (c), (d) Eigenstate distribution of $S_{\text{OPDM}}^{\text{min}}$ and $S_{\text{OPDM}}^{\text{max}}$, respectively. Data are averaged over 10^4 disorder realization and are obtained from $6 \cdot 10^4$ eigenstates. Results are for fixed $\epsilon = 1, V/J = 1, W/J = 15$, and system size $L = 16$.

$S_{\text{OPDM}}^{\text{max}}$ as

$$S_{\text{OPDM}}^{\text{min}} = \min(S_{\text{OPDM}}(A), S_{\text{OPDM}}(\bar{A})) \quad (6)$$

$$S_{\text{OPDM}}^{\text{max}} = \max(S_{\text{OPDM}}(A), S_{\text{OPDM}}(\bar{A})). \quad (7)$$

Figures 1(c) and (d) show the respective typical distributions in eigenstates. Clearly, $P(S_{\text{OPDM}}^{\text{min}})$ is the closest to $P(S_{\text{vN}})$ as it exhibits the smallest tails at large values. Therefore, we expect that $S_{\text{OPDM}}^{\text{min}}$ is the best candidate to capture the scaling properties of the von-Neumann entropy, which will be substantiated by the following analysis.

VI. AREA LAW OF THE OPDM ENTROPY IN THE MBL REGIME

In this section, we show that for the eigenstates of (1), the disorder-averaged OPDM entropy defined in Eq. (6) satisfies the area law. This behavior can be anticipated from the limit of strong disorder, i.e., deep in the MBL phase. In this limit, the eigenvalues of the OPDM take the values $n_\alpha = 0, 1$, i.e., they exhibit the typical step-like behavior as for free-fermion systems. This signals that the MBL-localized state is close to a single Slater determinant [34, 35], for which the OPDM entropy coincides with the von-Neumann entropy. Since this proximity to a Slater determinant persists throughout the MBL regime and since the eigenmodes of the OPDM are a proxy for the localized quasiparticles [35], it is natural to expect that for sufficiently strong disorder, the OPDM entropy (5) exhibits a similar behavior as the von-Neumann entropy.

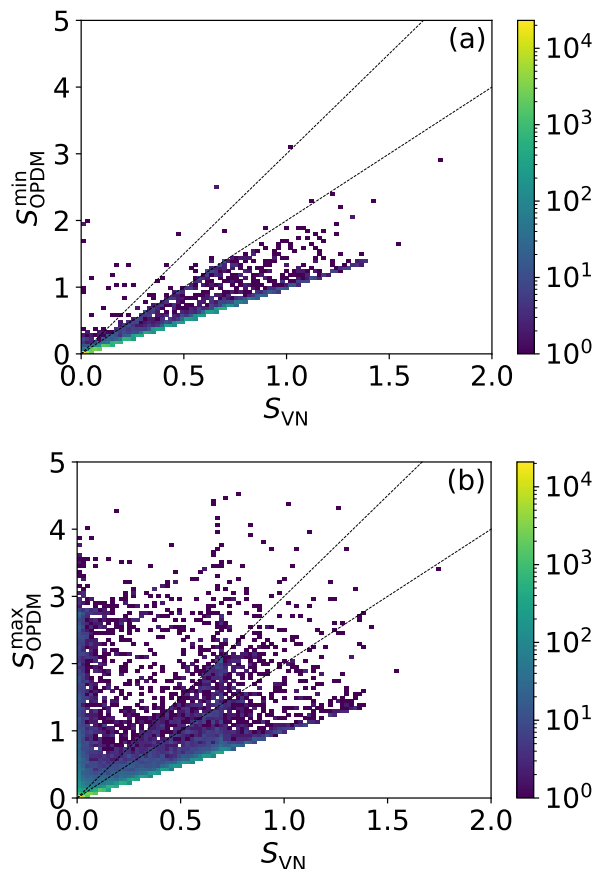


FIG. 2. (a) 2D histogram showing the correlation between von-Neumann entanglement entropy S_{vN} and the OPDM entropy $S_{\text{OPDM}}^{\text{min}}$, both computed in the same eigenstate. For each pair of $(S_{\text{vN}}, S_{\text{OPDM}}^{\text{min}})$, the color encodes the number of eigenstates with those entropies. Data are averaged over 10^4 disorder realizations and are obtained from $6 \cdot 10^4$ eigenstates. Results are for fixed $\epsilon = 1, V/J = 1, W/J = 15$, and system size $L = 16$. (b) The same for $S_{\text{OPDM}}^{\text{max}}$. Thin dotted lines indicate $S = 2S_{\text{vN}}$ and $S = 3S_{\text{vN}}$.

In Fig. 2(a), we focus on the half-chain entanglement entropy and OPDM entropy for a system with $L = 16$. Results are for $V/J = 1$ and $W/J = 15$. For these parameters, the system is expected to be in the MBL phase because the putative transition happens at $W_c/J \approx 4$ [34, 36, 54–56]. Note also that for $V/J = 1$, the system is far from the “trivial” non-interacting limit $V = 0$.

The 2D histogram shows the correlation between S_{vN} (on the x -axis) and $S_{\text{OPDM}}^{\text{min}}$ (on the y -axis) computed in the same eigenstate. The color scale denotes the number of eigenstates with a given pair of values of the entanglement entropies. The main conclusion from Fig. 2(a) is that the OPDM entropy is always larger than the entanglement entropy, i.e., $S_{\text{vN}} \leq S_{\text{OPDM}}^{\text{min}}$ for all eigenstates. This is a confirmation of the results of Ref. [50], yet for a many-body system. One can also observe that the majority of the points lies close to the diagonal, i.e., for most of the eigenstates, S_{vN} is close to $S_{\text{OPDM}}^{\text{min}}$. Interestingly, a

second cluster of states is visible at $S_{\text{OPDM}}^{\text{min}} = 2S_{\text{vN}}$. This feature corresponds to resonant pairs and is explained below. With increasing disorder strength, at least for fixed system size, all eigenstates collapse on the main diagonal and the minimal OPDM entropy becomes comparable to the von-Neumann entropy. In the limit of strong disorder $W/J \rightarrow \infty$, the eigenstates become single Slater determinants for which the equality holds.

For comparison, in Fig. 2(b), we show the half-chain entanglement entropy and the maximal OPDM entropy $S_{\text{OPDM}}^{\text{max}}$ for the same systems considered in Fig. 2(a). Here, one also observes some points that are close to the diagonal and a second cluster of states is visible at $S_{\text{OPDM}}^{\text{max}} = 2S_{\text{vN}}$. Moreover, a third diagonal emerges along $S_{\text{OPDM}}^{\text{max}} = 3S_{\text{vN}}$ and, more importantly, there are states for which $S_{\text{OPDM}}^{\text{max}} \gg S_{\text{vN}} \approx 0$. These features render $S_{\text{OPDM}}^{\text{min}}$ the better object to capture the scaling properties of S_{vN} as compared to $S_{\text{OPDM}}^{\text{max}}$.

We now explain, using a toy two-particle system of 4 sites, that the second diagonal in Figs. 2(a) and (b) is due to interactions. Let us consider a two-particle state

$$|\psi\rangle = \sum_{\alpha\beta} \psi_{\alpha\beta} |\alpha, \beta\rangle = \sum_{\alpha\beta} \psi_{\alpha\beta} c_{\alpha}^{\dagger} c_{\beta}^{\dagger} |0\rangle \quad (8)$$

where $|0\rangle$ is the fermionic vacuum and the creation operator c_{α}^{\dagger} creates a fermion in a localized state α (this can be a site, i.e., a Wannier orbital). Here, we assume that site $\alpha \in \{1, 2\}$ is in subsystem A whereas site $\beta \in \{3, 4\}$ is in \bar{A} . Such a state $|\psi\rangle$ assumes each fermion to be localized in the respective parts and neglects fluctuations of the fermions across the boundary (for states accounting for the fluctuations, see Appendix A). We note that the particular choice for $|\psi\rangle$ with all $\psi_{\alpha\beta} = 1/2$ was considered in Ref. [25] as a toy model for localized particles in an initial product state to understand the out-of-equilibrium dynamics of the von-Neumann entropy. There, it was shown that effective interactions between localized particles induce a growth of the von-Neumann entropy in time.

In those states that are described by Eq. (8), any (effective) interaction gives rise to correlations between the fermions resulting in non-trivial eigenstates. A nontrivial eigenstate that can be generated is a state close to the superposition $|\psi'\rangle = \psi_{13}|1, 3\rangle + \psi_{24}|2, 4\rangle$. It is straightforward to check that for $|\psi'\rangle$, the correlation matrix $C^{(A)}$ and the reduced density matrix $\rho^{(A)}$ for subsystem A coincide and are diagonal as

$$\rho^{(A)} = C^{(A)} = \begin{pmatrix} |\psi_{13}|^2 & 0 \\ 0 & 1 - |\psi_{13}|^2 \end{pmatrix} \quad (9)$$

where we used the normalization condition $|\psi_{24}|^2 = 1 - |\psi_{13}|^2$. For our two-particle system, the same applies to $C^{(\bar{A})}$ and $\rho^{(\bar{A})}$ which implies that $S_{\text{OPDM}}^A = S_{\text{OPDM}}^{\bar{A}}$ and thus $S_{\text{OPDM}}^{\text{min}} = S_{\text{OPDM}}^{\text{max}}$. It is thus sufficient to consider one number S_{OPDM} only. By varying the coefficient ψ_{13} one obtains $0 \leq S_{\text{vN}} \leq \ln(2)$. It is also straightforward to check that for any ψ_{13} , $S_{\text{OPDM}} = 2S_{\text{vN}}$.

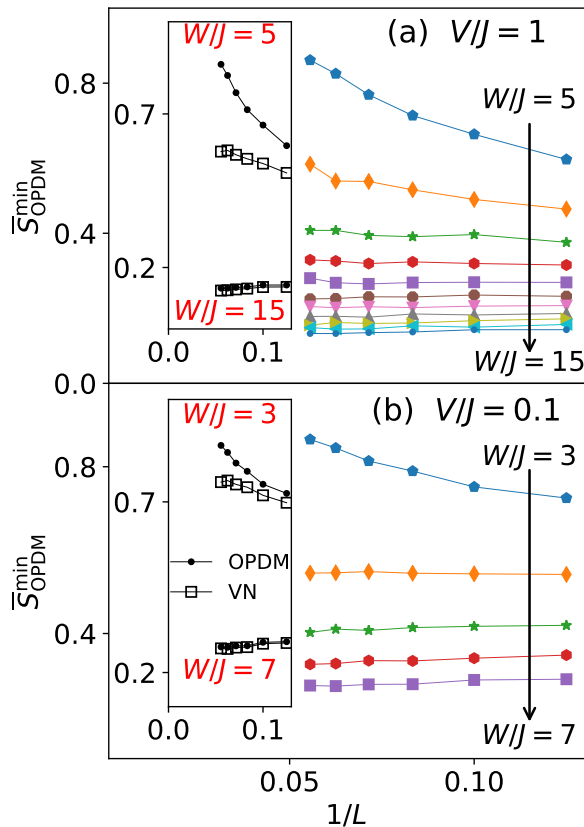


FIG. 3. (a): Main panel: Disorder average of the OPDM entropy $\bar{S}_{\text{OPDM}}^{\text{min}}$ plotted as a function of $1/L$ for $V/J = 1$ and disorder strength $W/J = 5, \dots, 15$ (different symbols). The arrow shows increasing disorder strength. Inset: Comparison between OPDM entropy $\bar{S}_{\text{OPDM}}^{\text{min}}$ (full circles) and von-Neumann entropy \bar{S}_{vN} (open squares) for $V/J = 1$ and $W/J = 5, 15$. (b): Same as in (a) for weak interactions $V/J = 0.1$ and disorder strength $W/J = 3, \dots, 7$.

Several remarks are in order. First, the reasoning laid out above is not expected to capture the full entanglement patterns in Figs. 2(a) and (b). For instance, in general, a third diagonal with eigenstates with $S_{\text{OPDM}} = 3S_{\text{vN}}$ can appear, see Fig. 2(b). This requires taking into account more complicated correlations involving more than two fermions. Still, the clustering of the eigenstates around the main and the second diagonal suggests that the entanglement structure is dominated by correlations involving two-body resonances across the boundary between the two subsystems.

We now demonstrate that the *disorder-averaged* OPDM entropy $\bar{S}_{\text{OPDM}}^{\text{min}}$ obeys the area law (the L -dependence of $\bar{S}_{\text{OPDM}}^{\text{max}}$ is discussed in Appendix B). In Fig. 3, we present the average OPDM entropy for the half chain as a function of L for several values of W/J and for $V/J = 1$ and for $V/J = 0.1$. For $V/J = 1$, standard diagnostic tools give a putative MBL transition at $W_c/J \approx 4$ [34, 36, 54–56] (see also [57–67]). In Fig. 3(a), we display the L -dependence of the OPDM

entropy on the MBL side. Deep in the MBL phase (for instance, for $W/J \geq 10$), the OPDM entropy is almost L -independent, implying area-law behavior [20–22]. Moreover, the OPDM entropy becomes very close to the von-Neumann entropy upon increasing the disorder strength [see the inset of Fig. 3(a)]. For the regime of weak interactions $V/J = 0.1$ [see Fig. 3(b)], smaller values of W are sufficient to observe the area-law behavior. This is expected because upon lowering V , the MBL transition is shifted towards smaller values of W . We estimate the transition at $V = 0.1J$ from standard diagnostic tools, such as the average gap ratio [36, 68] and the occupation distance measure [56], which give $W_c/J \approx 2 - 3$ (see Appendix C). An analysis of the behavior of $\bar{S}_{\text{OPDM}}^{\text{min}}$ across the transition into the ergodic region is beyond the scope of the present work and left for future research.

VII. LOGARITHMIC GROWTH OF THE OPDM ENTROPY IN THE MBL REGIME

Next, we discuss the time-dependence of the OPDM entropy after a global quantum quench deep in the MBL phase. We consider the evolution from initial random product states such as $|\psi_0\rangle = |1010\dots 1\rangle$, where 0, 1 are the initial fermionic occupations. We study the Hamiltonian dynamics $|\psi(t)\rangle = e^{-iHt}|\psi_0\rangle$ by using full exact diagonalization of H . For each disorder configuration, we select product states $|\psi_0\rangle$ with energy density $\epsilon = (\langle\psi_0|H|\psi_0\rangle - E_{\text{min}})/(E_{\text{max}} - E_{\text{min}})$ that fulfills $|1/2 - \epsilon| \lesssim 2 \cdot 10^{-4}$, i.e., close to mid-spectrum energy density. We average over 200 disorder realizations.

In the putative MBL phase, the von-Neumann entropy grows logarithmically after global quenches [23–25, 69], whereas on the ergodic side, a ballistic or sub-ballistic entanglement growth is observed [70]. The change of behavior happens at the eigenstate transition [69]. As anticipated in Sec. III, after a quantum quench, we observe $S_{\text{OPDM}}(t) \geq S_{\text{vN}}(t)$ in all states at any time.

First, we provide a simple argument why the OPDM entropy increases logarithmically after a quantum quench from initial product state. Let us again consider a generic state in Eq. (8). We take a particular choice of this state, where all $\psi_{\alpha\beta} = 1/2$, and follow the arguments of Ref. [25]. The initial state can be written as $|\psi_0\rangle = \frac{1}{2}(c_1^\dagger + c_2^\dagger)(c_3^\dagger + c_4^\dagger)|0\rangle$. For such initial state, there is no entanglement between the particle in orbitals 1, 2 and the particle in orbitals 3, 4 at $t = 0$ as can be verified by a direct calculation. An effective interaction produces the time-evolved state $|\psi(t)\rangle$, which is given by

$$|\psi(t)\rangle = \sum_{\alpha,\beta} \frac{1}{2} e^{-iE_{\alpha\beta}t} |\alpha, \beta\rangle, \quad (10)$$

where the energies $E_{\alpha\beta}$ are $E_{\alpha\beta} = \epsilon_\alpha + \epsilon_\beta + \delta E_{\alpha\beta}$ and ϵ_α and ϵ_β are the single-particle energies, whereas $\delta E_{\alpha\beta}$ is due to the interactions. It is natural to expect that $\delta E_{\alpha\beta} = k_{\alpha\beta} \tilde{V} e^{-x/\xi}$, with $k_{\alpha\beta}$ a constant, \tilde{V} an effective

interaction strength between the two localized particles with distance x from each other, and ξ the localization length, for which we assume $x \gg \xi$. For the state from Eq. (10), the reduced density matrix $\rho^{(A)}$ coincides with the OPDM matrix $C^{(A)}$ and is given by

$$\rho^{(A)} = C^{(A)} = \frac{1}{2} \begin{pmatrix} 1 & F(t)/2 \\ F^*(t)/2 & 1 \end{pmatrix}, \quad (11)$$

where $F(t) = e^{-i\Omega t}(1 + e^{-i\delta\Omega t})$, with $\Omega = \epsilon_1 - \epsilon_2 + \delta E_{13} - \delta E_{23}$ and $\delta\Omega = \delta E_{14} - \delta E_{24} + \delta E_{13} + \delta E_{23}$. The eigenvalues of $\rho^{(A)}$ are

$$\lambda_{\pm} = \frac{1}{2} \left(1 \pm \frac{|F(t)|}{2} \right). \quad (12)$$

Note that $F(t)$ vanishes at $t^* = \pi/\delta\Omega$ and at $t^* = \pi/2\delta\Omega$, the entanglement entropy S_{vN} has a maximum with $S_{\text{vN}} = \ln(2)$. This effect is due to $\delta\Omega$, which reflects the presence of (effective) interactions. By using the definition of the OPDM entropy, one obtains that $S_{\text{OPDM}}(t) = 2S_{\text{vN}}(t)$. Therefore, at any time, the OPDM entropy differs from the von-Neumann entropy only by a pre-factor. This pre-factor can in general be different from 2 because the toy state in Eq. (10) does not account for the full correlation pattern of a general many-body wave function.

In Fig. 4(a), we show the dynamics of the OPDM entropy $\bar{S}_{\text{OPDM}}^{\text{min}}$ for $V/J = 1$ (strong interactions) and $W/J = 5, \dots, 15$ and for $V/J = 0.1$ (weak interactions) and $W/J = 3, \dots, 7$ computed numerically for $L = 16$ (the time dependence of $\bar{S}_{\text{OPDM}}^{\text{max}}$ is discussed in Appendix B). In both cases, the system is in the MBL phase. For large enough times, the data exhibit a clear logarithmic increase for all values of W . The prefactor of the logarithmic growth depends on the interaction strength V , and hence is non-universal, as for the von-Neumann entropy. Note that in the limit $W/J \rightarrow \infty$, the entropy saturates. Interestingly, the prefactors of the logarithmic growth of the OPDM entropy and of the von-Neumann entropy are not the same. This is illustrated in the insets of Fig 4. Only in the limit of large W/J , the dynamics of the OPDM entropy becomes quantitatively the same as the von-Neumann entropy.

Finally, interesting features appear for weak interactions [see Fig. 4(b)]. First, longer times are needed for the logarithmic behavior to set in. For instance, for $V/J = 0.1$, this happens for $tJ \geq 100$. Moreover, the dynamics of the OPDM entropy and that of the von-Neumann entropy is the same at short times. This is highlighted in the insets in Fig. 4. Clearly, the OPDM entropy coincides with the von-Neumann entropy up to $tJ \approx 10$.

VIII. CONCLUSIONS

We provided numerical evidence that the OPDM entropy exhibits the salient features of the von-Neumann

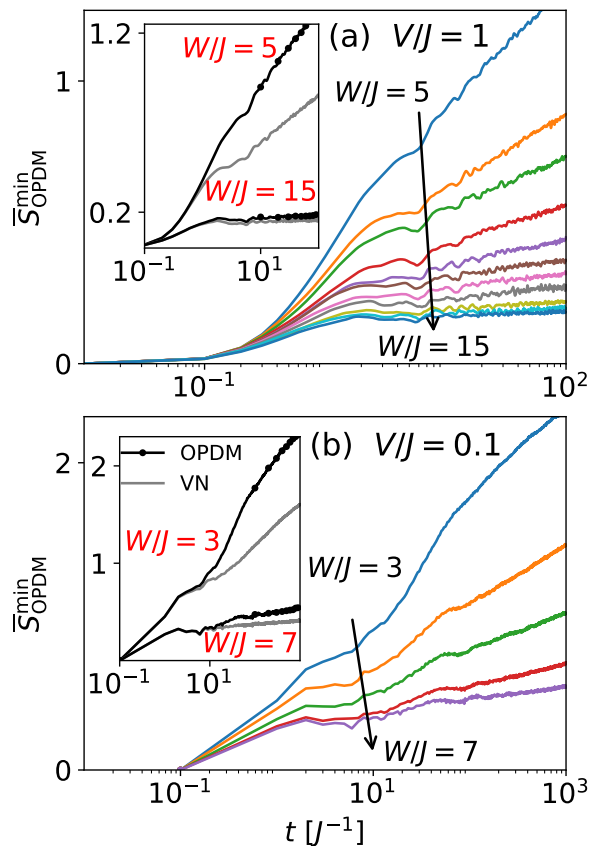


FIG. 4. (a): Main panel: Time evolution of the average OPDM entropy $\bar{S}_{\text{OPDM}}^{\text{min}}$ for $L = 16$, $V/J = 1$ and disorder strength $W/J = 5, \dots, 15$. The arrow denotes increasing disorder strength. For all values of W , a clear logarithmic growth with a non-universal prefactor is visible at long times. Inset: Comparison between the OPDM entropy $\bar{S}_{\text{OPDM}}^{\text{min}}$ (full circles) and the von-Neumann entropy \bar{S}_{vN} (gray lines) for $L = 16$, $V/J = 1$ and $W/J = 5, 15$. (b) Same as in (a) for weak interactions $V/J = 0.1$ and disorder strength $W/J = 3, \dots, 7$.

entropy in putative MBL phases of matter. Specifically, deep in MBL phases, the eigenstate OPDM entropy obeys the area law. Most importantly, the entropy grows logarithmically after a global quantum quench. Although formally, this is expected in the limit $W/J \rightarrow \infty$, we observe that there is a sizeable region in parameter space, i.e., interaction and disorder strength, where this behavior persists. This behavior is expected since the OPDM eigenstates approximate the localized quasiparticles aka l-bits in the MBL phase [35].

There are several interesting directions for future work. First, our results could be combined with *ab-initio* methods for the correlation functions, e.g., Green's function methods [48, 71, 72]. This would allow to compute the evolution of the OPDM entropy for larger systems, and also in higher dimensions. Importantly, the computation of the OPDM scales only polynomial in the linear dimension. Moreover, it would be interesting to measure the evolution of the OPDM entropy in cold-atom

experiments using single-site resolution [13, 73, 74] or in embryonic quantum computers [75, 76]. Finally, in contrast with the entanglement entropy, the OPDM entropy relies on the fermionic correlation functions, which are standard tools in condensed matter physics. This renders the OPDM amenable to an analytical study and, for instance, by using the renormalization-group techniques reviewed in Ref. 1.

ACKNOWLEDGMENTS

We acknowledge useful discussions with J. H. Bardarson.

Appendix A: OPDM versus von-Neumann entropy in a two-particle, four-site system

In this section, we compare the OPDM and the von-Neumann entropy in a generic 2-particle fermionic state in a 4-site system with bipartition $A = \{1, 2\}$ and $\bar{A} = \{3, 4\}$. Note that for such system $S_{\text{OPDM}}^A = S_{\text{OPDM}}^{\bar{A}}$ and it is thus sufficient to consider one number S_{OPDM} only. Particles can be thought of as localized in A or as being delocalized across the boundary between A and \bar{A} . With this setup, we consider a generic wavefunction

$$|\psi\rangle = \sum_{\alpha < \beta} \psi_{\alpha\beta} |\alpha, \beta\rangle = \sum_{\alpha < \beta} \psi_{\alpha\beta} c_{\alpha}^{\dagger} c_{\beta}^{\dagger} |0\rangle, \quad (\text{A1})$$

where $|0\rangle$ is the fermionic vacuum and the creation operator c_{α}^{\dagger} creates a fermion at site α . We allow for particle fluctuations across the partition, i.e., $\alpha \in \{1, 2, 3\}$ and $\beta \in \{2, 3, 4\}$. The state in Eq. (A1) is a generalization of the state in Eq. (8) discussed in the main text. For such state, the matrix elements of $C^{(A)}$ read

$$C_{11}^{(A)} = |\psi_{12}|^2 + |\psi_{13}|^2 + |\psi_{14}|^2, \quad (\text{A2})$$

$$C_{22}^{(A)} = |\psi_{24}|^2 + |\psi_{23}|^2 + |\psi_{12}|^2, \quad (\text{A3})$$

$$C_{12}^{(A)} = \psi_{14}^* \psi_{24} + \psi_{13}^* \psi_{23}, \quad (\text{A4})$$

$$C_{21}^{(A)} = (C_{12}^{(A)})^*, \quad (\text{A5})$$

and the reduced density matrix reads

$$\rho^{(A)} = \begin{pmatrix} |\psi_{12}|^2 & 0 & 0 & 0 \\ 0 & C_{11}^{(A)} - |\psi_{12}|^2 & C_{12}^{(A)} & 0 \\ 0 & C_{21}^{(A)} & C_{22}^{(A)} - |\psi_{12}|^2 & 0 \\ 0 & 0 & 0 & |\psi_{34}|^2 \end{pmatrix}. \quad (\text{A6})$$

From (A6) and (A2)-(A5) one can construct the OPDM entropy and the entanglement entropy.

Neglecting particle fluctuations across the partition, i.e., setting $\psi_{12} = \psi_{34} = 0$, the OPDM coincides with the reduced density matrix $\rho^{(A)} = C^{(A)}$ and is given by

$$\rho^{(A)} = \begin{pmatrix} |\psi_{13}|^2 + |\psi_{14}|^2 & \psi_{14}^* \psi_{24} + \psi_{13}^* \psi_{23} \\ \psi_{24}^* \psi_{14} + \psi_{23}^* \psi_{13} & |\psi_{24}|^2 + |\psi_{23}|^2 \end{pmatrix}. \quad (\text{A7})$$

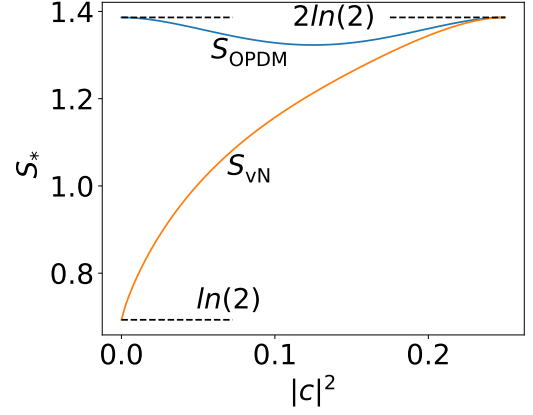


FIG. 5. Comparison between the von-Neumann and the OPDM entropy for the two-fermions states in (A10) as a function of $|c|^2$. Notice that $S_{\text{vN}} = 2S_{\text{OPDM}}$ for $|c| = 0$ and $S_{\text{vN}} = S_{\text{OPDM}}$ for $|c| = 1/2$. The horizontal dotted lines mark the values $\ln(2)$ and $2\ln(2)$.

A special case of the reduced density matrix in Eq. (A7) was given in the main text in Eq. (9) for which it was shown that $S_{\text{OPDM}} = 2S_{\text{vN}}$.

We will now discuss the clean system of 2 fermions in 4 sites with translational invariance. Here, there are 2 relevant state. The first one is the state $|\psi'\rangle$ from Eq. (8) with $|\psi_{13}|^2 = |\psi_{24}|^2$ which is translational invariant and can be written as

$$|\psi'\rangle = \sum_{\alpha=1}^2 \psi_{\alpha\alpha+2} |\alpha, \alpha+2\rangle, \quad (\text{A8})$$

for which we derive that $S_{\text{OPDM}} = 2S_{\text{vN}}$ in the main text. The second relevant state can be written as

$$|\psi''\rangle = \sum_{\alpha=1}^4 \psi_{\alpha\alpha+1} |\alpha, \alpha+1\rangle, \quad (\text{A9})$$

where $|\psi_{12}|^2 = |\psi_{23}|^2 = |\psi_{34}|^2 = |\psi_{14}|^2 = 1/2$ and we assume the periodic boundary conditions. Now the reduced density matrix is diagonal in the basis with four eigenvalues $1/4$, giving the von-Neumann entropy $S_{\text{vN}} = 2\ln(2)$. At the same time, the OPDM matrix is diagonal with two equal eigenvalues $1/2$, which give $S_{\text{OPDM}} = 2\ln(2)$. This confirms our expectation that for a maximally entangled state, the two entropies have to be equal.

The eigenstates of clean systems can be thought of as a mixture of the states in Eq. (A1) and Eq. (A9)

$$|\tilde{\psi}\rangle = \sum_{\alpha=1}^2 \psi_{\alpha\alpha+2} |\alpha, \alpha+2\rangle + \sum_{\alpha=1}^4 \psi_{\alpha\alpha+1} |\alpha, \alpha+1\rangle, \quad (\text{A10})$$

where $|\psi_{12}|^2 = |\psi_{23}|^2 = |\psi_{34}|^2 = |\psi_{14}|^2 =: |c|^2$ and $|\psi_{13}|^2 = |\psi_{24}|^2 =: |c'|^2$. Here, due to the normalization condition, we have $|c'|^2 = (1 - 4|c|^2)/2$. From (A6) and (A2)-(A5), one can obtain the entanglement entropy

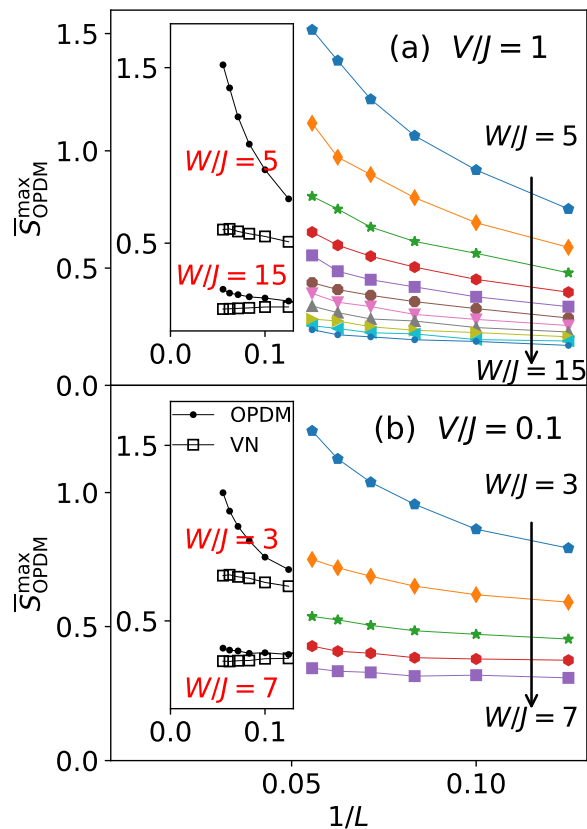


FIG. 6. (a): Main panel: Disorder average of the OPDM entropy $\bar{S}_{\text{OPDM}}^{\text{max}}$ plotted as a function of $1/L$ for $V/J = 1$ and disorder strength $W/J = 5, \dots, 15$ (different symbols). The arrow shows increasing disorder strength. Inset: Comparison between $\bar{S}_{\text{OPDM}}^{\text{max}}$ (full circles) and von-Neumann entropy \bar{S}_{vN} (open squares) for $V/J = 1$ and $W/J = 5, 15$. (b): Same as in (a) for weak interactions $V/J = 0.1$ and disorder strength $W/J = 3, \dots, 7$.

and the OPDM entropy as a function of $|c|^2$. In Fig. 5, we plot S_{vN} and S_{OPDM} as a function of $|c|^2$ assuming that both c and c' are real. As is clear from the figure, $S_{\text{OPDM}} \geq S_{\text{vN}}$ for any $|c|$. We thus see how the entropies interpolate between states $|\psi'\rangle$ and $|\psi''\rangle$.

Appendix B: Scaling of $\bar{S}_{\text{OPDM}}^{\text{max}}$

For comparison to the behavior of $\bar{S}_{\text{OPDM}}^{\text{min}}$ shown in Fig. 3, in Fig. 6, we show the average OPDM entropy $\bar{S}_{\text{OPDM}}^{\text{max}}$ for the half chain as a function of L and for several values of disorder strength W/J . On the one hand, deep in the MBL phase, e.g., at $W/J \approx 15$ for $V/J = 1$ [see Fig. 6(a)], the behavior of $\bar{S}_{\text{OPDM}}^{\text{max}}$ is similar to that of $\bar{S}_{\text{OPDM}}^{\text{min}}$ and $\bar{S}_{\text{OPDM}}^{\text{max}}$. On the other hand, $\bar{S}_{\text{OPDM}}^{\text{max}}$ is closer to the von-Neumann entropy than $\bar{S}_{\text{OPDM}}^{\text{min}}$ as displayed in the insets of Figs. 3 and 6. This is expected since $\bar{S}_{\text{OPDM}}^{\text{max}}$ includes more resonances across the two subsystems than

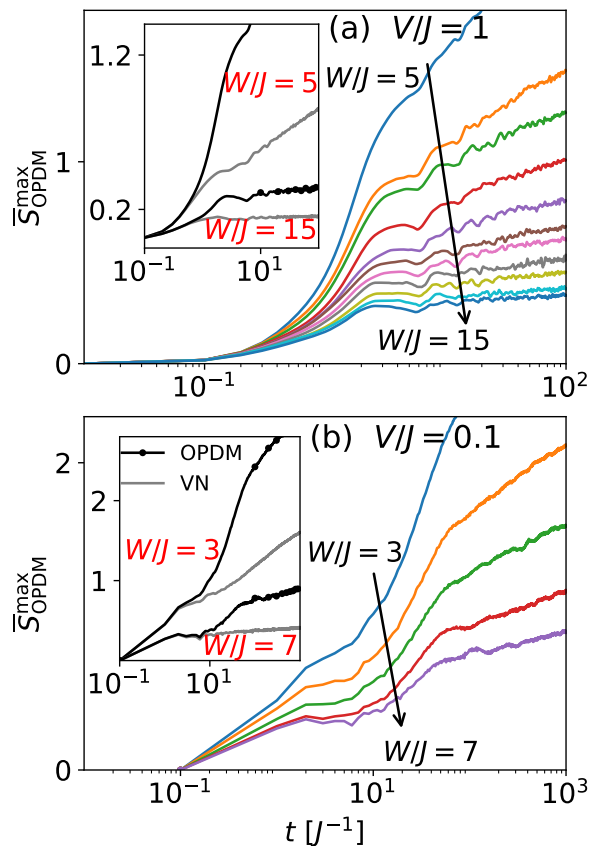


FIG. 7. (a): Main panel: Time evolution of the average OPDM entropy $\bar{S}_{\text{OPDM}}^{\text{max}}$ for $L = 16, V/J = 1$ and disorder strength $W/J = 5, \dots, 15$. The arrow denotes increasing disorder strength. For all values of W , a clear logarithmic growth with a non-universal prefactor is visible at long times. Inset: Comparison between $\bar{S}_{\text{OPDM}}^{\text{max}}$ (full circles) and the von-Neumann entropy \bar{S}_{vN} (gray lines) for $L = 16, V/J = 1$ and $W/J = 5, 15$. Note that the prefactor of the logarithmic growth of the OPDM entropy and of the von-Neumann entropy are different. (b) Same as in (a) for weak interactions $V/J = 0.1$ and disorder strength $W/J = 3, \dots, 7$.

$\bar{S}_{\text{OPDM}}^{\text{min}}$

In Fig. 7, we show the time evolution of $\bar{S}_{\text{OPDM}}^{\text{max}}$ for the same set of parameters as for $\bar{S}_{\text{OPDM}}^{\text{min}}$ in Fig. 4. As is clear from the figure, $\bar{S}_{\text{OPDM}}^{\text{max}}$ grows logarithmically with time after the quench. In the insets of Fig. 7, we compare $\bar{S}_{\text{OPDM}}^{\text{max}}$ and the von-Neumann entropy. Clearly, both entropies exhibit a logarithmic growth but with a different non-universal prefactor. Nevertheless, as in the case of eigenstates, we observe that $\bar{S}_{\text{OPDM}}^{\text{min}}$ compares better than $\bar{S}_{\text{OPDM}}^{\text{max}}$ to the von-Neumann entropy as displayed in the insets of Figs. 4 and 7.

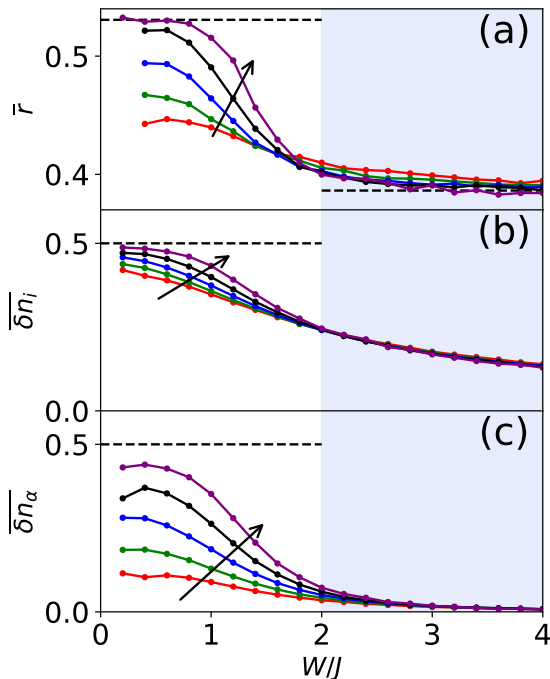


FIG. 8. Diagnostics of the MBL transition at $V/J = 0.1$: (a) average gap ratio \bar{r} , (b) average occupation distances $\overline{\delta n_i}$, (c) and $\overline{\delta n_\alpha}$. W/J , plotted on the horizontal axis is the disorder strength. We show data for $V/J = 0.1$. Different curves correspond to different system sizes $L = 10, 12, 14, 16, 18$. Data are averaged over up to 10^5 disorder realization. The arrows denote increasing system size. In (a), the horizontal dashed lines denote the analytic results assuming Wigner-Dyson ($\bar{r} \approx 0.53$) and Poisson distribution ($\bar{r} \approx 0.38$) of the energy level spacings. In (b), the occupation distances are expected to attain the values $\overline{\delta n_i} = 1/2$ in the ergodic phase (dashed lines). In all panels, the shaded area is estimated to be in the MBL phase. Thus, all results shown in the main text are for a disorder strength well above the transition.

Appendix C: MBL transition estimate and additional numerical data for weak interactions

In this section, we employ standard diagnostic tools to identify the putative MBL transition at $V/J = 0.1$ (see the main text). Specifically, we consider the average gap ratio [36, 68] and the occupation distance measure [56].

We start discussing the average gap ratio \bar{r} . Given the eigenenergies E_n of the quantum many-body Hamiltonian,

we first define the gaps δ_n as

$$\delta_n \equiv E_{n+1} - E_n. \quad (\text{C1})$$

The gap ratio r_n is defined as

$$0 \leq r_n = \min\{\delta_n, \delta_{n-1}\} / \max\{\delta_n, \delta_{n-1}\} \leq 1. \quad (\text{C2})$$

The average ratio \bar{r} results from averaging over the eigenstates of the Hamiltonian and over disorder configurations. For Poisson-distributed energy-level spacings, e.g., for integrable systems, the average value of the ratio is $\bar{r} = 2 \ln(2) - 1 \approx 0.386$. In the non-integrable case, one expects that level spacings are described by the Gaussian Orthogonal Ensemble (GOE) [77]. This yields $\bar{r} = 4 - 2\sqrt{3} \approx 0.535$ for 3×3 matrices.

In Fig. 8 (a), we show \bar{r} [36, 68] as a function of W/J . The expected behavior [36, 68] is visible. At weak disorder, \bar{r} converges to the GOE result upon increasing L while in the strong-disorder regime, \bar{r} is compatible with the Poisson value $\bar{r} \approx 0.38$. Using the scaling ansatz form $\bar{r} = g(L^{1/\nu}(W - W_c))$ [36], with ν a critical exponent and W_c the critical value of the disorder, we get $W_c/J = 2.0(2)$ (we have used $L = 14, 16, 18$ for the scaling collapse). However, similar to Ref. [36], one obtains $\nu = 0.6(1)$, which violates the Harris bound [60, 78, 79]. In conclusion, the analysis of the gap ratio \bar{r} suggests a change in behavior at $W_c/J \approx 2$.

To complement our analysis, we also consider the occupation distances δn_i and δn_α introduced in Ref. [56]. These are derived from the OPDM

$$\rho_{ij}^{(1)} = \langle \psi_n | c_i^\dagger c_j | \psi_n \rangle, \quad (\text{C3})$$

where $|\psi_n\rangle$ denotes an eigenstate. We define n_i as the fermionic spatial occupations $n_i = \rho_{ii}^{(1)}$, and n_α are the eigenvalues of $\rho_{ij}^{(1)}$. Here, we consider the distances $\delta n_i = n_i - [n_i]$ and $\delta n_\alpha = n_\alpha - [n_\alpha]$ to the closest integers of $[n_i]$ and $[n_\alpha]$, respectively. Finally, we obtain the averaged occupation distances $\overline{\delta n_i}$ and $\overline{\delta n_\alpha}$ by averaging over different disorder realizations.

The occupation distances measure the degree of Fock-space localization in the chosen single-particle basis. They are almost independent of system size in the MBL phase [56], while in the ergodic region, $\overline{\delta n_i}$ must converge to the average particle filling, in our case 0.5, while $\overline{\delta n_\alpha}$ approaches a smaller, energy-dependent value.

In Figs. 8(b) and (c), we plot the occupation distances $\overline{\delta n_i}$ and $\overline{\delta n_\alpha}$ as a function of W/J . We observe that $\overline{\delta n_i}$ become almost L -independent for $W/J > 2$. For $\overline{\delta n_\alpha}$, this happens for $W/J > 2.6$. Thus, the occupation distances confirm the qualitative scenario obtained from the analysis of the gap ratio \bar{r} [see Fig. 8(a)].

[1] E. Altman and R. Vosk, *Ann. Rev. Cond. Matt. Phys.* **6**, 383 (2015).

[2] R. Nandkishore and D. A. Huse, *Ann. Rev. Cond. Matt. Phys.* **6**, 15 (2015).

- [3] E. Altman, *Nat. Phys.* **14**, 979 (2018).
- [4] F. Alet and N. Laflorencie, *C. R. Phys.* **19**, 498 (2018).
- [5] D. A. Abanin, E. Altman, I. Bloch, and M. Serbyn, *Rev. Mod. Phys.* **91**, 021001 (2019).
- [6] P. W. Anderson, *Phys. Rev.* **109**, 1492 (1958).
- [7] I. V. Gornyi, A. D. Mirlin, and D. G. Polyakov, *Phys. Rev. Lett.* **95**, 206603 (2005).
- [8] D. Basko, I. Aleiner, and B. Altshuler, *Ann. Phys. (N.Y.)* **321**, 1126 (2006).
- [9] J. Smith, A. Lee, P. Richerme, B. Neyenhuis, P. W. Hess, P. Hauke, M. Heyl, D. A. Huse, and C. Monroe, *Nat. Phys.* **12**, 907 (2016).
- [10] J.-Y. Choi, S. Hild, J. Zeiher, P. Schauß, A. Rubio-Abadal, T. Yefsah, V. Khemani, D. A. Huse, I. Bloch, and C. Gross, *Science* **352**, 1547 (2016).
- [11] M. Schreiber, S. S. Hodgman, P. Bordia, H. P. Lüschen, M. H. Fischer, R. Vosk, E. Altman, U. Schneider, and I. Bloch, *Science* **349**, 842 (2015).
- [12] M. Rispoli, A. Lukin, R. Schittko, S. Kim, M. E. Tai, J. Léonard, and M. Greiner, *Nature* **573**, 385 (2019).
- [13] A. Lukin, M. Rispoli, R. Schittko, M. E. Tai, A. M. Kaufman, S. Choi, V. Khemani, J. Léonard, and M. Greiner, *Science* **364**, 256 (2019).
- [14] A. Rubio-Abadal, J.-Y. Choi, J. Zeiher, S. Hollerith, J. Rui, I. Bloch, and C. Gross, *Phys. Rev. X* **9**, 041014 (2019).
- [15] K. Xu, J.-J. Chen, Y. Zeng, Y.-R. Zhang, C. Song, W. Liu, Q. Guo, P. Zhang, D. Xu, H. Deng, K. Huang, H. Wang, X. Zhu, D. Zheng, and H. Fan, *Phys. Rev. Lett.* **120**, 050507 (2018).
- [16] P. Roushan, C. Neill, J. Tangpanitanon, V. M. Bastidas, A. Megrant, R. Barends, Y. Chen, Z. Chen, B. Chiaro, A. Dunsworth, A. Fowler, B. Foxen, M. Giustina, E. Jeffrey, J. Kelly, E. Lucero, J. Mutus, M. Neeley, C. Quintana, D. Sank, A. Vainsencher, J. Wenner, T. White, H. Neven, D. G. Angelakis, and J. Martinis, *Science* **358**, 1175 (2017).
- [17] B. Chiaro, C. Neill, A. Bohrdt, M. Filippone, F. Arute, K. Arya, R. Babbush, D. Bacon, J. Bardin, R. Barends, S. Boixo, D. Buell, B. Burkett, Y. Chen, Z. Chen, R. Collins, A. Dunsworth, E. Farhi, A. Fowler, B. Foxen, C. Gidney, M. Giustina, M. Harrigan, T. Huang, S. Isakov, E. Jeffrey, Z. Jiang, D. Kafri, K. Kechedzhi, J. Kelly, P. Klimov, A. Korotkov, F. Kostritsa, D. Landhuis, E. Lucero, J. McClean, X. Mi, A. Megrant, M. Mohseni, J. Mutus, M. McEwen, O. Naaman, M. Neeley, M. Niu, A. Petukhov, C. Quintana, N. Rubin, D. Sank, K. Satzinger, A. Vainsencher, T. White, Z. Yao, P. Yeh, A. Zalcman, V. Smelyanskiy, H. Neven, S. Gopalakrishnan, D. Abanin, M. Knap, J. Martinis, and P. Roushan, [arXiv:1910.06024](https://arxiv.org/abs/1910.06024).
- [18] Q. Guo, C. Cheng, Z.-H. Sun, Z. Song, H. Li, Z. Wang, W. Ren, H. Dong, D. Zheng, Y.-R. Zhang, R. Mondaini, H. Fan, and H. Wang, *Nat. Phys.* (2020), [10.1038/s41567-020-1035-1](https://doi.org/10.1038/s41567-020-1035-1).
- [19] T. Kohlert, S. Scherg, X. Li, H. P. Lüschen, S. Das Sarma, I. Bloch, and M. Aidelsburger, *Phys. Rev. Lett.* **122**, 170403 (2019).
- [20] B. Bauer and C. Nayak, *J. Stat. Mech. Theor. Exp.* **2013**, P09005 (2013).
- [21] J. A. Kjäll, J. H. Bardarson, and F. Pollmann, *Phys. Rev. Lett.* **113**, 107204 (2014).
- [22] M. Friesdorf, A. H. Werner, W. Brown, V. B. Scholz, and J. Eisert, *Phys. Rev. Lett.* **114**, 170505 (2015).
- [23] M. Žnidarič, T. Prosen, and P. Prelovšek, *Phys. Rev. B* **77**, 064426 (2008).
- [24] J. H. Bardarson, F. Pollmann, and J. E. Moore, *Phys. Rev. Lett.* **109**, 017202 (2012).
- [25] M. Serbyn, Z. Papić, and D. A. Abanin, *Phys. Rev. Lett.* **110**, 260601 (2013).
- [26] Y. Huang, (2021), [10.20944/preprints202104.0254.v1](https://arxiv.org/abs/2010.20944).
- [27] P. Calabrese and J. Cardy, *Journal of Statistical Mechanics: Theory and Experiment* **2005**, P04010 (2005).
- [28] G. D. Chiara, S. Montangero, P. Calabrese, and R. Fazio, *J. Stat. Mech.: Theory and Experiment* **2006**, P03001 (2006).
- [29] M. Fagotti and P. Calabrese, *Phys. Rev. A* **78**, 010306 (2008).
- [30] V. Alba and P. Calabrese, *Proceedings of the National Academy of Sciences* **114**, 7947 (2017).
- [31] D. A. Huse, R. Nandkishore, and V. Oganesyan, *Phys. Rev. B* **90**, 174202 (2014).
- [32] J. Z. Imbrie, V. Ros, and A. Scardicchio, *Ann. Phys. (Leipzig)* **529**, 1600278 (2017).
- [33] J. Z. Imbrie, *Phys. Rev. Lett.* **117**, 027201 (2016).
- [34] S. Bera, H. Schomerus, F. Heidrich-Meisner, and J. H. Bardarson, *Phys. Rev. Lett.* **115**, 046603 (2015).
- [35] S. Bera, T. Martynek, H. Schomerus, F. Heidrich-Meisner, and J. H. Bardarson, *Ann. Phys. (Leipzig)* **529**, 1600356 (2017).
- [36] D. J. Luitz, N. Laflorencie, and F. Alet, *Phys. Rev. B* **91**, 081103 (2015).
- [37] S. Roy, J. T. Chalker, and D. E. Logan, *Phys. Rev. B* **99**, 104206 (2019).
- [38] D. E. Logan and S. Welsh, *Phys. Rev. B* **99**, 045131 (2019).
- [39] T. L. M. Lezama, S. Bera, H. Schomerus, F. Heidrich-Meisner, and J. H. Bardarson, *Phys. Rev. B* **96**, 060202 (2017).
- [40] S.-H. Lin, B. Sbierski, F. Dorfner, C. Karrasch, and F. Heidrich-Meisner, *SciPost Phys.* **4**, 002 (2018).
- [41] W. Buijsman, V. Gritsev, and V. Cheianov, *SciPost Phys.* **4**, 38 (2018).
- [42] B. Villalonga, X. Yu, D. J. Luitz, and B. K. Clark, *Phys. Rev. B* **97**, 104406 (2018).
- [43] C. P. Chen, M. Szyniszewski, and H. Schomerus, *Phys. Rev. Research* **2**, 023118 (2020).
- [44] I. Peschel and V. Eisler, *Journal of Physics A: Mathematical and Theoretical* **42**, 504003 (2009).
- [45] J. I. Latorre and A. Riera, *Journal of Physics A: Mathematical and Theoretical* **42**, 504002 (2009).
- [46] S. Thomsson and M. Schiró, *Phys. Rev. B* **97**, 060201 (2018).
- [47] G. De Tomasi, F. Pollmann, and M. Heyl, *Phys. Rev. B* **99**, 241114 (2019).
- [48] S. A. Weidinger, S. Gopalakrishnan, and M. Knap, *Phys. Rev. B* **98**, 224205 (2018).
- [49] G. De Tomasi, S. Bera, J. H. Bardarson, and F. Pollmann, *Phys. Rev. Lett.* **118**, 016804 (2017).
- [50] E. Greplová and G. Giedke, *Phys. Rev. Lett.* **121**, 200501 (2018).
- [51] A. S. Holevo, M. Sohma, and O. Hirota, *Phys. Rev. A* **59**, 1820 (1999).
- [52] M. M. Wolf, G. Giedke, and J. I. Cirac, *Phys. Rev. Lett.* **96**, 080502 (2006).
- [53] F. Pietracaprina, N. Macé, D. J. Luitz, and F. Alet, *SciPost Phys.* **5**, 45 (2018).
- [54] N. Macé, F. Alet, and N. Laflorencie, *Phys. Rev. Lett.*

- 123**, 180601 (2019).
- [55] N. Laflorencie, G. Lemarié, and N. Macé, *Phys. Rev. Research* **2**, 042033 (2020).
- [56] M. Hopjan and F. Heidrich-Meisner, *Phys. Rev. A* **101**, 063617 (2020).
- [57] T. Devakul and R. R. P. Singh, *Phys. Rev. Lett.* **115**, 187201 (2015).
- [58] E. V. H. Doggen, F. Schindler, K. S. Tikhonov, A. D. Mirlin, T. Neupert, D. G. Polyakov, and I. V. Gornyi, *Phys. Rev. B* **98**, 174202 (2018).
- [59] T. Chanda, P. Sierant, and J. Zakrzewski, *Phys. Rev. B* **101**, 035148 (2020).
- [60] V. Khemani, D. N. Sheng, and D. A. Huse, *Phys. Rev. Lett.* **119**, 075702 (2017).
- [61] J. Šuntajs, J. Bonča, T. Prosen, and L. Vidmar, *Phys. Rev. E* **102**, 062144 (2020).
- [62] P. Sierant, D. Delande, and J. Zakrzewski, *Phys. Rev. Lett.* **124**, 186601 (2020).
- [63] D. Abanin, J. Bardarson, G. De Tomasi, S. Gopalakrishnan, V. Khemani, S. Parameswaran, F. Pollmann, A. Potter, M. Serbyn, and R. Vasseur, *Annals of Physics* **427**, 168415 (2021).
- [64] R. K. Panda, A. Scardicchio, M. Schulz, S. R. Taylor, and M. Žnidarič, *EPL* **128**, 67003 (2019).
- [65] T. Chanda, P. Sierant, and J. Zakrzewski, *Phys. Rev. Research* **2**, 032045 (2020).
- [66] J. Šuntajs, J. Bonča, T. Prosen, and L. Vidmar, *Phys. Rev. B* **102**, 064207 (2020).
- [67] P. Sierant, M. Lewenstein, and J. Zakrzewski, *Phys. Rev. Lett.* **125**, 156601 (2020).
- [68] V. Oganesyan and D. A. Huse, *Phys. Rev. B* **75**, 155111 (2007).
- [69] M. Serbyn, Z. Papić, and D. A. Abanin, *Phys. Rev. X* **5**, 041047 (2015).
- [70] D. J. Luitz, N. Laflorencie, and F. Alet, *Phys. Rev. B* **93**, 060201 (2016).
- [71] Y. Bar Lev and D. R. Reichman, *Phys. Rev. B* **89**, 220201 (2014).
- [72] Y. B. Lev and D. R. Reichman, *EPL (Europhysics Letters)* **113**, 46001 (2016).
- [73] J. F. Sherson, C. Weitenberg, M. Endres, M. Cheneau, I. Bloch, and S. Kuhr, *Nature* **467**, 68 (2010).
- [74] L. A. Peña Ardila, M. Heyl, and A. Eckardt, *Phys. Rev. Lett.* **121**, 260401 (2018).
- [75] F. Arute, K. Arya, R. Babbush, D. Bacon, J. Bardin, R. Barends, R. Biswas, S. Boixo, F. Brandao, D. Buell, B. Burkett, Y. Chen, J. Chen, B. Chiaro, R. Collins, W. Courtney, A. Dunsworth, E. Farhi, B. Foxen, A. Fowler, C. M. Gidney, M. Giustina, R. Graff, K. Guerin, S. Habegger, M. Harrigan, M. Hartmann, A. Ho, M. R. Hoffmann, T. Huang, T. Humble, S. Isakov, E. Jeffrey, Z. Jiang, D. Kafri, K. Kechedzhi, J. Kelly, P. Klimov, S. Knysh, A. Korotkov, F. Kostritsa, D. Landhuis, M. Lindmark, E. Lucero, D. Lyakh, S. Mandrà, J. R. McClean, M. McEwen, A. Megrant, X. Mi, K. Michielsen, M. Mohseni, J. Mutus, O. Naaman, M. Neeley, C. Neill, M. Y. Niu, E. Ostby, A. Petukhov, J. Platt, C. Quintana, E. G. Rieffel, P. Roushan, N. Rubin, D. Sank, K. J. Satzinger, V. Smelyanskiy, K. J. Sung, M. Trevithick, A. Vainsencher, B. Villalonga, T. White, Z. J. Yao, P. Yeh, A. Zalcman, H. Neven, and J. Martinis, *Nature* **574**, 505–510 (2019).
- [76] A. Smith, M. Kim, F. Pollmann, and J. Knolle, *npj Quantum Information* **5**, 1 (2019).
- [77] L. D'Alessio, Y. Kafri, A. Polkovnikov, and M. Rigol, *Adv. Phys.* **65**, 239 (2016).
- [78] A. B. Harris, *Journal of Physics C: Solid State Physics* **7**, 1671 (1974).
- [79] A. Chandran, C. R. Laumann, and V. Oganesyan, [arXiv:1509.04285](https://arxiv.org/abs/1509.04285).